Experimental studies of necking and fracture limits of boron steel sheet under hot stamping conditions

Ruiqiang Zhang, Zhusheng Shi, Victoria A. Yardley * and Jianguo Lin

Department of Mechanical Engineering, Imperial College London, London SW7 2AZ, UK

* Corresponding author: v.yardley@imperial.ac.uk (V. Yardley).

Abstract

Boron steel is the most widely used material in hot stamping applications for forming automotive body panels with complex shapes and ultra-high strength. Due to the high austenitic transformation temperatures and the complex thermal cycle required for hot stamping, however, it is difficult to evaluate the formability of the material using standard punch test methods developed for room-temperature testing. In this study, a high-temperature modification of a recently developed biaxial test method has been used to determine, in a single test procedure and for the first time, forming limit curves (FLCs) and fracture forming limit curves (FFLCs) for 22MnB5 boron steel sheet with a thickness of 1.5 mm under thermal conditions that are representative of industrial hot stamping processes. A direct resistance heating strategy has been developed, and a recently proposed cruciform specimen design has been modified for high-temperature use. For tests with target temperatures in the range of 750 to 925 °C, the resulting test specimens had the highest temperature at the specimen centre and a temperature difference of less than 45 °C in the gauge area and fracture occurred close to the centre of this area under all test conditions investigated. Limit strains at the onset of necking and at fracture for the material have been determined by applying digital image correlation (DIC) to obtain full-field strain measurements, providing an experimental foundation for constructing both FLCs and FFLCs for industrial applications.

Keywords: Biaxial testing; Cruciform specimen; Formability; Boron steel; Hot stamping; Forming limit curve (FLC); Fracture forming limit curve (FFLC);

1. Introduction

Hot stamping, also called hot forming or press hardening, is widely used in industry to form lightweight parts, where complex shapes and ultra-high strength are required (Karbasian and Tekkaya, 2010). Hot stamped boron steel sheet is one of the main materials used in safety-critical automotive parts (Merklein et al., 2016); its use has become widespread in the vehicles launched onto the market in recent years (e.g. Bachman (2018)). In the hot stamping process, boron steels are held above the Ae_3 temperature (around 900 °C) for a long enough time to obtain a homogeneous austenitic microstructure (Merklein and Lechler, 2006); the steels are transferred to water-cooled forming tools within several seconds, then formed and quenched simultaneously. With the increasing use of hot-stamped steel components in lightweight vehicles, characterising the formability of boron steel under these conditions has become essential for controlling the final product quality and evaluating the success of the sheet forming operation (Turetta et al., 2006).

Forming limit curves (FLCs), originally proposed by Keeler (1965) and Goodwin (1968) are the most widely accepted tools for the assessment of the formability of metallic materials. They are generated by plotting the necking limits, i.e. the major strain at the onset of localised necking, ε_1, against the corresponding minor strain ε_2 (Raghavan, 1995). A complementary tool for formability evaluation, which may be preferred over FLCs in certain applications, is fracture forming limit curves or FFLCs (Atkins, 1996). These are plotted using the fracture limits, i.e. the major and minor strains at the onset of fracture (Jawale et al., 2018). The most popular methods for the determination of FLCs and FFLCs at room temperature are the Nakajima and Marciniak tests; here, waisted specimens are clamped between a blank holder and a die, and are deformed to fracture using a hemispherical punch in the Nakajima test (Nakazima et al., 1968) and a flat punch in the Marciniak test (Marciniak and

Kuczyński, 1967). It is worth mentioning that, in both the Nakajima (Li et al., 2020) and the Marciniak tests (Wang et al., 2014), a suitable lubricant system must be used between the punch and the specimens in order to initiate failure near to the specimen centre (i.e. within a distance less than 15% of the punch diameter), since the test is only valid in this case. Formability evaluation using either the Nakajima or the Marciniak procedure has been standardised in the international standard ISO 12004-2 (BS EN ISO 12004, 2008). These test methods have also been used for the evaluation of formability of sheet metals at high temperatures (Palumbo et al., 2008); for this, specimens must be held at the required temperatures throughout deformation. One method of achieving this is to install the testing tools such as the punch, die and specimen holder in a furnace and carry out the test within it (Bruni et al., 2010). An alternative approach is to preheat the tools and then allow them to heat the specimens by thermal conduction during the test (Ma et al., 2016). However, it is difficult to evaluate the formability of boron steel at hot stamping temperatures using either the Nakajima or the Marciniak procedure (Min et al., 2010b). One reason for this difficulty is that the high temperatures required to austenitise the material before stamping cause the failure of the lubricant systems between the punch and the specimens (Li et al., 2014). The other is that the complex heat treatment route used in the hot stamping of boron steel cannot be precisely reproduced using existing methods for high-temperature Nakajima or Marciniak testing (Bariani et al., 2008).

Biaxial test methods using cruciform specimens (BS ISO 16842, 2014) represent an alternative approach to high-temperature formability evaluation, and their potential has already been demonstrated (Xiao, 2019). In this approach, the specimen is heated to its target temperature and maintained at this temperature while being stretched to failure under a state of plane stress using a biaxial testing system (Hannon and Tiernan, 2008), together with a system for measuring strain fields and a method for determining limit strains (Leotoing et al., 2013). Using a biaxial tensile testing machine equipped with a furnace for heating specimens described by Xiao et al. (2016), Xiao et al. (2017) determined FLCs for a TA1 titanium alloy sheet of thickness 1 mm at a range of temperatures

from 25 to 800 °C. Shao et al. (2016) designed and patented a new biaxial tensile rig which was assembled in a Gleeble thermal-mechanical simulator, enabling in-situ heating during testing, and evaluated FLCs for an AA6082 aluminium alloy sheet with a thickness of 1.5 mm at hot stamping temperatures over a range of 400 to 500 °C. Chen et al. (2020) determined FFLCs for an AA7075 sheet with a thickness of 1.8 mm at 480 °C. A major advantage of biaxial test methods is that, unlike in the Nakajima test, there is no need to use lubricant systems (Güler and Efe, 2018), so the problems caused by the failure of the lubricants at high temperatures in the Nakajima test, such as initiation of fracture at undesirable locations, can be avoided. Due to the lack of a widely accepted cruciform specimen design enabling linear strain paths to be generated at the site where fracture initiates (Zidane et al., 2010) and a suitable method for determining the necking and fracture limits (Min et al., 2017a; Min et al., 2017b), however, biaxial test methods have not been commonly used for formability assessment even at room temperature.

In a recent study (Zhang et al., 2021c), a biaxial test method which comprised a cruciform specimen geometry (Zhang et al., 2021a), a biaxial testing system for straining cruciform specimens under plane stress (Shao et al., 2016), and a spatio-temporal method for measuring both the necking and fracture limits (Zhang et al., 2021b) was successfully applied to generate an FLC and an FFLC in the same test procedure for an AA5754 sheet with a thickness of 1.5 mm at room temperature. This biaxial test method was validated by comparing the necking limits obtained with this method against those obtained using the standard Nakajima method (Zhang et al., 2021c). One of the challenges when applying this biaxial method to the formability assessment of boron steel at hot stamping temperatures is reproducing the heat-treatment histories used in industrial hot stamping processes (Farhadzadeh et al., 2018). In their previous study, Shao et al. (2016) demonstrated that heating the cruciform specimens using a direct resistance heating system in a Gleeble thermal-mechanical simulator before and during stretching using the patented biaxial rig allowed industrially relevant thermomechanical cycles to be replicated. According to the numerical simulation result presented in Fig. A3 of Appendix

A, however, the direct resistance heating method applied to the existing cruciform specimens gives maxima of temperature at positions outside the gauge region, such that it is highly unlikely that fracture would be initiated at the specimen centre. It is therefore not possible to apply the method in its existing form (Zhang et al., 2021c) to high-temperature testing without modifications to the test methodology.

The aim of the present study is to extend the application of the recently developed biaxial test method (Zhang et al., 2021c) to high temperatures, using the results to construct both FLCs and FFLCs for a 22MnB5 boron steel sheet with a thickness of 1.5 mm at hot stamping temperatures. A new direct resistance heating strategy is used to heat the boron steel specimens. The recent specimen design is modified to increase the temperature at the specimen centre relative to that in the other regions and hence to enable the fracture to be initiated near the centre of the specimen under all test conditions, and to produce a more uniform temperature distribution within the specimen gauge area. Biaxial tensile tests at hot stamping temperatures are carried out on the boron steel sheet under different conditions of strain state, temperature and strain rate. Digital image correlation (DIC) is applied to measure the full-field strains within the specimen gauge area. Both the necking and fracture limits are determined, and FLCs and FFLCs for the material are constructed and discussed.

2. Methodology

2.1. Material and hot stamping thermal cycle

Zinc-coated boron steel (22MnB5) sheet with an initial thickness of 1.5 mm was used in the present study. The material had the chemical composition Fe-0.20C-1.17Mn-0.25Si-0.20Cr-0.002S-0.0029B-0.028Ti-0.001Nb-0.023Ni (wt. %). Fig. 1 shows an illustrative thermal cycle used in this study to mimic industrial hot stamping conditions for boron steel (Zhang et al., 2020). The material was heated from room temperature to 875 °C at an initial constant heating rate of 10 °C/s, then a lower heating rate of 5 °C/s was used to heat to 925 °C to avoid temperature overshoot. After soaking

at 925 °C, which is above the Ae_3 temperature (i.e. 850-900 °C) for this material (Li et al., 2016), for 60 s to ensure full transformation to austenite, the material was air quenched at a constant rate of 60 °C/s to the forming temperature T_F, which takes a value between Ae_1 (i.e. 700-750 °C) and Ae_3, such as the value of 800 °C shown in Fig. 1.

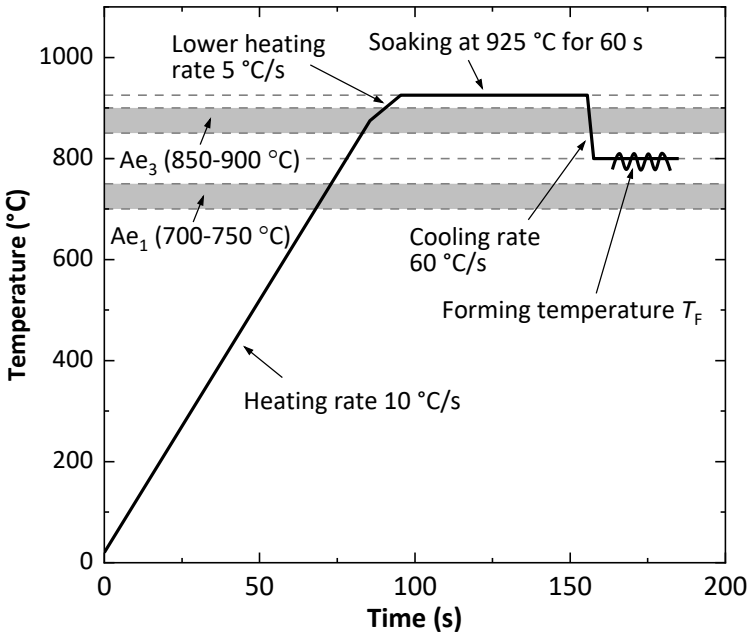

Fig. 1. Temperature profile used in the present study to mimic industrial hot stamping (Zhang et al., 2020).

2.2. Modified biaxial test method for formability assessment at high temperature

The recently developed biaxial test method, which was demonstrated to be capable of determining formability (i.e. both FLCs and FFLCs) at room temperature (Zhang et al., 2021c), is modified and applied in the present work to determine the formability of materials at the high temperatures associated with hot stamping. This modified method is schematically illustrated in Fig. 2, in which a Gleeble thermal-mechanical simulator equipped with a direct resistance heating system is used to provide multi-step heat treatments such as those shown in Fig. 1 (Zhang et al., 2020). The biaxial tensile system consists of the Gleeble and the biaxial tensile rig. In the same way as in room-temperature testing, the slider-crank mechanisms of the biaxial tensile rig convert the uniaxial force provided by the Gleeble to the biaxial forces needed for straining cruciform specimens in plane stress.

The spatio-temporal method (Zhang et al., 2021b) is used to analyse the full-field strains, measured using the DIC method, of the cruciform specimen throughout deformation, and to obtain the necking and fracture limit strain pairs (ε_2, ε_1); these are necessary to generate FLCs and FFLCs, respectively.

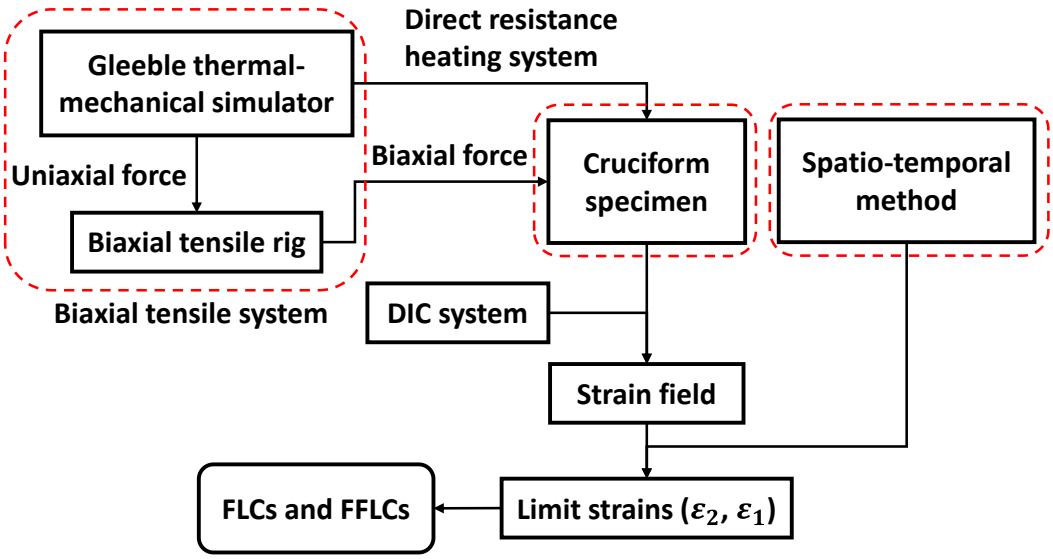

Fig. 2. Schematic of the modified biaxial test method for determining both FLCs and FFLCs at high temperature. The biaxial test method consists of three main parts (circled with dashed red lines), i.e. the biaxial tensile system to provide direct resistance heating and biaxial force, the cruciform specimen to produce various strain states, and the spatio-temporal method to obtain the necking and fracture limit strain pairs (ε_2, ε_1), where ε_1 is the limit major strain and ε_2 is the associated minor strain.

2.3. Experimental programme

2.3.1. Direct resistance heating strategy and modified cruciform specimen design

The heating strategy used in the present work is illustrated in Fig. 3; the upper arm is connected to the positive electrode of the direct resistance heating system and the lower arm is connected to the negative electrode. To give greater uniformity in temperature within the gauge region, the cruciform specimen design that was used for room-temperature testing (Zhang et al., 2021c) has been modified; these modifications are (1) removing the slits in the vertical arms, (2) reducing the distance $D_{\mathrm{S-V}}$ between two opposite slits in the horizontal arms from 20 to 17.5 mm, (3) increasing the distance D_{F} between two adjacent arm notches from 20 to 26 mm, and (4) increasing the number N_{S} of slits in

each horizontal arm from 2 to 4, to give the design shown in Fig. 3. The reason for removing the slits in the vertical arms is to increase the stiffness of the vertical arms in the arm notches. The reason for reducing D_{S-V} and increasing D_F is to decrease the cross-sectional area, through which the current flows in the vertical direction, of the central thinned region (e.g. Section IV-IV in Fig. 3) relative to that of the vertical arms near the arm notches (e.g. Section III-III), and thus to enable higher temperatures to develop in the central thinned region than in other regions, particularly in the vertical arm notches. The increase of N_S is to reduce the lateral stiffness of the horizontal arms to compensate for the increase in lateral stiffness that would otherwise be caused by increasing D_F. Fig. 3 presents the modified cruciform specimen design used in the present study, together with the parametric dimensions; the values of these are given in Table 1. The thinned region, also called the thickness-reduced zone, contains a gauge area with diameter D_C, which is thinned using a dome profile of radius R_D through the thickness on only one side of the specimen. The other side of the specimen, which faces the camera in all the tests, is flat in the gauge area. The specimens used in the present study were thinned using computer numerical control (CNC) milling machines.

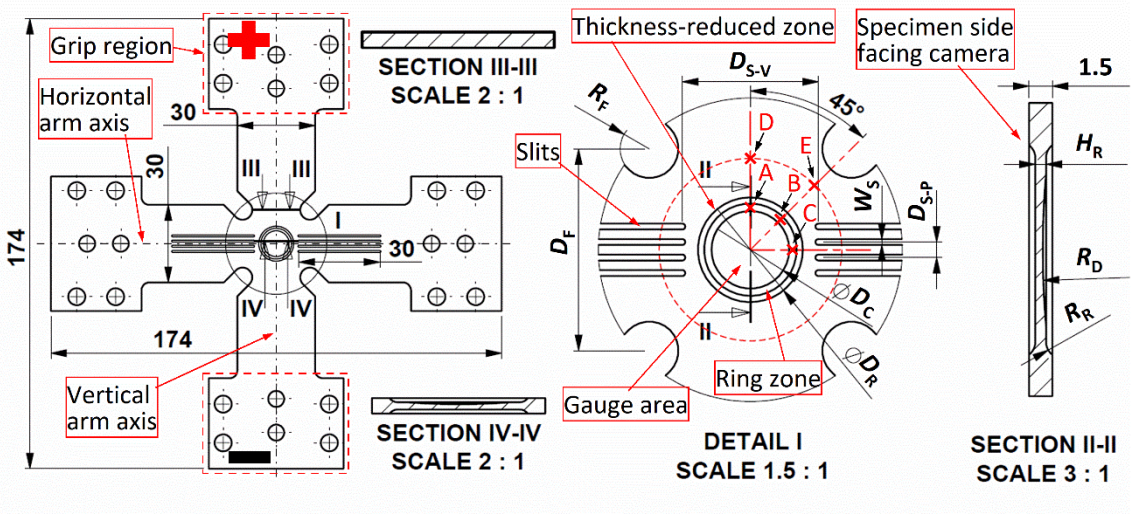

Fig. 3. Geometry and dimensions of the modified cruciform specimen design for formability tests on boron steel at hot stamping temperatures, showing locations A, B, C, D and E selected for experimental temperature measurement. The symbols '+' and '−' represent the connection of the grip regions to the positive and negative electrodes, respectively.

Table 1 Dimensions (in millimetre) of the modified cruciform specimen design.

Feature	Central area		Slits in arms				Thickness-reduced zone				
Dimension	D_{F}	R_{F}	N_{S}	$D_{\mathrm{S-V}}$	W_{S}	$D_{\mathrm{S-P}}$	D_{R}	H_{R}	R_{R}	D_{C}	R_{D}
Value	26	3.75	4	17.5	0.75	2	13.5	0.7	1	10	60

Due to the symmetrical boundary conditions, the temperature distribution in the specimens is expected to be symmetrical with respect to both the horizontal and the vertical arm axes (Fig. 3). To evaluate the temperature distribution during typical hot-stamping thermal cycles (Fig. 1), the temperature at the five locations A, B, C, D, and E, indicated in Fig. 3, as well as that at the centre, was experimentally measured using type K thermocouples. Of these locations, A, B, and C are in the ring zone and D and E on a circle of radius 11.75 mm centred on the specimen centre. Locations A and D lie on the vertical central axis and C on the horizontal central axis, while B and E are on a line through the centre at an angle of 45° to the vertical arm direction. Locations A, B and C are on the circumference of the gauge area and, together with the central thermocouple, are used to characterise the degree of temperature variation within the gauge area. In addition, these experimental temperature data were used to calibrate finite element (FE) simulations used in the development of the modified cruciform specimen and calculation of temperature distributions; details of the FE simulations can be found in Appendix A.

2.3.2. Test conditions

Considering the highly viscoplastic nature of the boron steel at hot stamping temperatures (Zhang et al., 2020), formability tests were carried out at temperatures from 750 to 850 °C and effective strain rates from 0.02 to 0.5 /s. The full set of conditions is given in Table 2. In order to construct whole FLCs and FFLCs, formability tests under each of the sets of conditions in Table 2 were conducted in three different strain states. Displacement ratios $\Delta y/\Delta x$ of 1, 0.2 and −0.17 were applied, where Δy

is the relative displacement of the specimen grips in the vertical arm direction and Δx that in the horizontal direction, and negative values represent compression in the vertical direction, with the aim of achieving equi-biaxial (β = 1), plane-strain (β = 0) and uniaxial (for isotropic materials, $\beta = -0.5$) strain states, respectively, where $\beta = \mathrm{d}\varepsilon_2/\mathrm{d}\varepsilon_1$ is the ratio of minor strain increment ($\mathrm{d}\varepsilon_2$) to major strain increment ($\mathrm{d}\varepsilon_1$). These displacement ratios were determined using trial and error and have been used in earlier room-temperature tests (Zhang et al., 2021c). It will be seen in Section 3.2 that the displacement ratios are different from the strain ratios. One reason for this is that the strain ratios are defined using true strain increments rather than engineering strain increments. The other reason is that the deformation within the specimen gauge area along both the vertical and horizontal arm directions is nonuniform, as will be seen in Section 3.2. At least two tests were carried out for each set of conditions. During high-temperature testing, a pair of thermocouples (Type K) was welded to the specimen centre to supply signals to enable accurate feedback control of the specimen temperature. The total force applied to the biaxial rig was measured using the load cell of the Gleeble during each test.

Table 2 Test conditions (indicted by ' √ ') for formability evaluation of the boron steel at hot stamping temperatures.

Temperature (°C)	Effective strain rate (/s)		
	0.02	0.1	0.5
750		√	
800	√	√	√
850		√	

2.3.3. Strain field measurement and limit strain determination from test specimens

The DIC technique was used in the present study to measure strain fields. The speckle patterns on the specimens were prepared using the method developed by some of the present authors (Zhang et al.,

2020). The thermomechanical tests were carried out in vacuum to avoid oxidation of the material. Images of the gauge area of the specimen were recorded throughout deformation using a high-speed camera with a frame rate determined for each effective strain rate by trial and error, namely, 50 frames per second (fps) for the tests at 0.02 /s, 250 fps at 0.1 /s, and 500 fps at 0.5 /s. Strain values were obtained from the images using the GOM Correlate software package (GOM, Germany) by setting facet size to 19 pixels and point distance to 10 pixels. In the recorded pictures, the gauge zone of the cruciform specimens had at least 3×10^5 pixels to ensure sufficient precision of the measured strain fields.

The spatio-temporal method to obtain both necking and fracture limit strains, developed by Zhang et al. (2021b), was used in the present work. The parameters introduced in the spatio-temporal method have the following values in the present study: $W_{\mathrm{BZ}} = 2 \times h_0$, $W_{\mathrm{RZ}} = 2 \times W_{\mathrm{BZ}}$, $W_{\mathrm{L}} = 2 \times h_0$, $t_{\mathrm{BN}} = 0.4 \times t_{\mathrm{F}}$, and $t_{\mathrm{AN}} = 0.998 \times t_{\mathrm{F}}$, where h_0 is the thickness of the test specimen before deformation.

3. Results

3.1. Temperature distributions

Fig. 4(a) shows the temperature histories measured at the centre and at locations A and C for a target forming temperature T_{F} of 750 °C; Fig. 4(b) shows the same curves for T_{F} = 850 °C. In both cases, the temperature histories measured at A and C closely follow that measured at the specimen centre, but are slightly shifted towards lower temperatures, the shift being more pronounced at C than at A. Fig. 4(a) also shows a photograph of the specimen (inset), taken approximately at the time marked on the curve. There is a change of colour from red to orange, yellow and white going from the edges to the central region of the specimen; this indicates an increase of temperature. The colours are symmetrically distributed about the specimen centre lines (horizontal and vertical), giving qualitative evidence that the temperature distribution is symmetrical about these lines, as is expected from the boundary conditions.

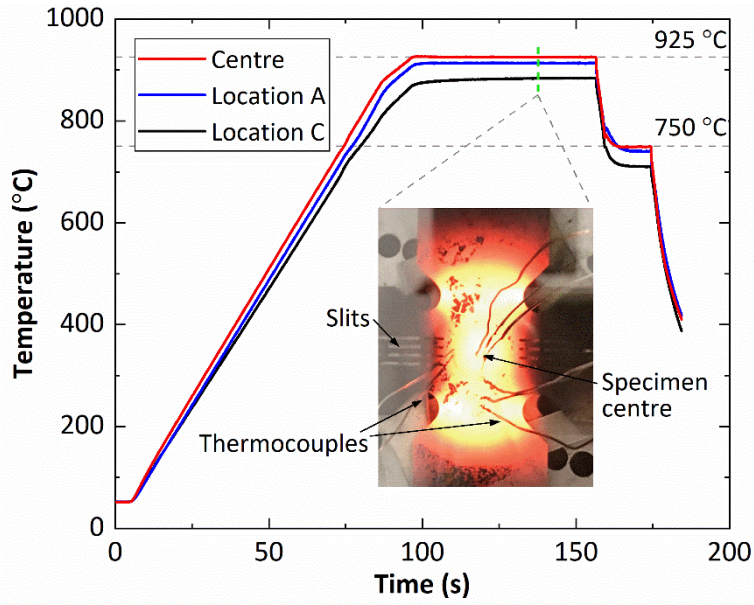

(a)

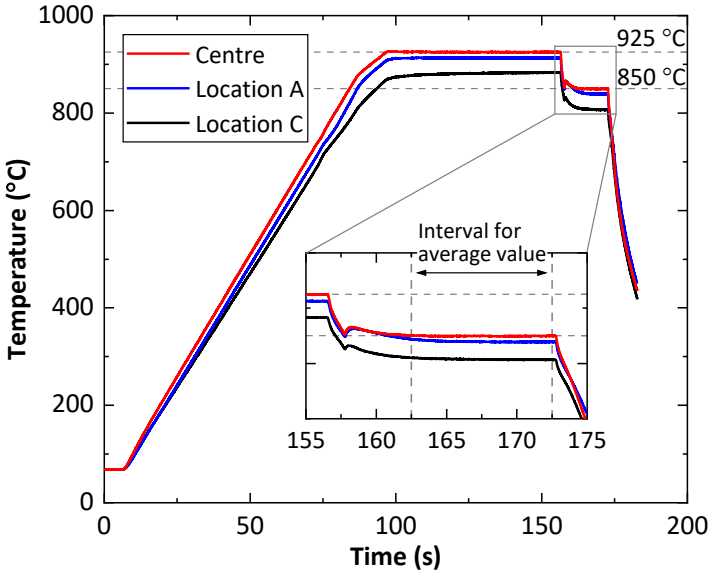

(b)

Fig. 4. Measured temperature histories at the specimen centre and at locations A and C, for target forming temperature T_F of (a) 750 °C and (b) 850 °C.

The mean temperature value for each thermocouple and condition was obtained from an interval over which the temperature was considered to have stabilised (inset in Fig. 4(b)). Table 3 presents the results for four different specimen centre temperatures, which were obtained by following the thermal cycle shown in Fig. 1: the first line of Table 3 is for the soaking temperature of 925 °C and the

following lines are for soaking at 925 °C followed by holding at the forming temperatures (T_F) of 850, 800 and 750 °C. Each test condition was repeated three times and the mean values of these repetitions were given in Table 3, together with the standard deviation *s*. Considering only the measurements made in the thinned zone, the temperature was higher at the specimen centre than at any of the locations A, B, C in all cases. The decrease in temperature from the specimen centre to these locations was greater in the horizontal arm direction (location C) than in the vertical (A) and diagonal (B) directions. When the specimen centre was at the target temperature of 925 °C, the temperature was 12 °C lower than this at location A, and 28 °C lower at B. The maximum decrease within the gauge area was less than 42 °C, only 2.6% of the absolute temperature (in K) at the specimen centre. Under the other three test conditions, similar temperature distributions were produced, and the maximum temperature variation within the gauge area was less than 43.2, 41.6 and 39.3 °C, respectively, namely less than 3.1% of the absolute temperature (K) at the specimen centre. This indicates that using this heating strategy (Fig. 3), in combination with the specimen design (Fig. 3 and Table 1), enables minimal temperature variation within the gauge area under the test conditions of interest. Regarding the temperatures measured further from the specimen centre, the value at E (diagonal) was much lower than that at the specimen centre in all cases. Although the temperature at D (vertical) was higher than that at the specimen centre for T_F = 750 and 800 °C, the maximum difference between D and the centre temperature was less than 8 °C.

Table 3 Mean measured temperatures (°C) and associated standard deviation *s* at locations A, B, C, D and E for different temperatures at the specimen centre.

Specimen centre	A	B	C	D	E
925.0	912.9 ± 0.4	896.6 ± 0.5	883.0 ± 0.7	914.9 ± 1.1	859.1 ± 0.9
850.0	838.8 ± 0.9	819.6 ± 0.4	806.8 ± 1.1	845.8 ± 1.0	786.7 ± 1.5
800.0	790.0 ± 0.7	770.4 ± 0.8	758.4 ± 0.7	801.2 ± 0.5	741.6 ± 1.6
750.0	740.4 ± 0.7	721.0 ± 0.7	710.7 ± 0.7	757.9 ± 1.1	696.7 ± 0.8

3.2. Practical biaxial tests on boron steel at hot stamping temperatures

3.2.1. Equi-biaxial tension

Fig. 5 shows photographs of fractured cruciform specimens of the boron steel after testing in equi-biaxial tension under the five different test conditions given in Table 2. In all the tests, fracture took place very close to the specimen centre and within the gauge area.

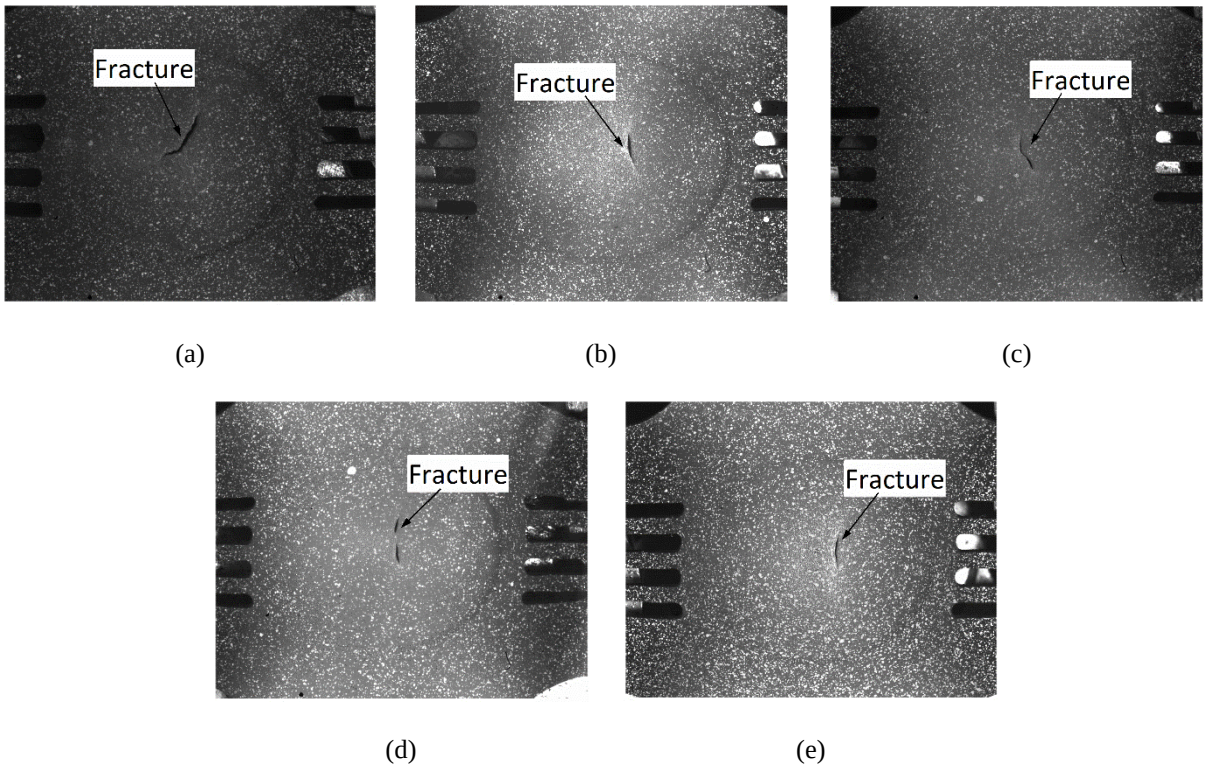

Fig. 5. Fractured boron steel cruciform specimens in equi-biaxial tension, under conditions (temperature and strain rate) of: (a) 750 °C & 0.1 /s, (b) 800 °C & 0.1 /s, (c) 850 °C & 0.1 /s, (d) 800 °C & 0.02 /s and (e) 800 °C & 0.5 /s.

Fig. 6 shows the determination, using the spatio-temporal method of Zhang et al. (2021b), of the limit strains for the equi-biaxial tensile test carried out at 800 °C and 0.1 /s, and the corresponding strain path. Fig. 6(a) presents the thickness reduction $|\varepsilon_3|$ in the thickness-reduced zone at the normalised times t/t_{F} = 0.9 and 1, where t_{F} is the time to fracture. A base zone (BZ) covering the immediate vicinity of the eventual crack site and a reference zone (RZ) covering a wider area were drawn around the fracture initiation site, such that the sides of the zones were parallel and perpendicular to the long axis of the crack (Fig. 5(b) for the 800 °C and 0.1 /s case). The initial specimen thickness near the

specimen centre (h_0), which is used to calculate the dimensions of the BZ and RZ (Section 2.3.3) was approximately 0.55 mm according to the specimen design (Fig. 3). Fig. 6(b) is a colour plot of the major strain ε_1. It can be seen that deformation has mainly taken place around the specimen centre. In Fig. 6(c), the average thickness reduction within the RZ is plotted versus that within the BZ. When deformation is uniform, the ratio between these quantities is ideally unity, but once necking begins, the average thickness reduction within the BZ becomes greater than that within the RZ, resulting in a change in slope in the plot of RZ versus BZ. Straight lines fitted using the least-squares method to experimental data (red dots) in the ranges $0 \leq t \leq t_{\mathrm{BN}}$ (green dashed line) and $t_{\mathrm{AN}} \leq t \leq t_{\mathrm{F}}$ (blue dashed line) are plotted in Fig. 6(c); the intersection of these lines corresponds to the onset of localised necking. The fracture time t_{F} is defined as the time immediately before the observation of a visible crack in the recorded pictures of the gauge area of the specimens. The times t_{BN} and t_{AN} used to define the datapoints used for fitting the straight lines, are determined from the fracture time using the formulae given in Section 2.3.3. The time corresponding to the intersection of the two fitted lines is the time t_{LN} of onset of localised necking. Fig. 6(d) is a plot of the major strain ε_1 against the minor strain ε_2 throughout deformation. The limit strain pair (ε_2, ε_1) at the time of localised necking t_{LN}, was found to be (0.153, 0.346) and the corresponding values at the time of fracture t_{F} were (0.234, 0.532). The strain path (plot of ε_1 against ε_2) is almost linear throughout deformation, while the strain ratio $\beta = \mathrm{d}\varepsilon_2/\mathrm{d}\varepsilon_1$ is about 0.45, which is considerably less than the ideal strain ratio of unity expected under equi-biaxial stretching.

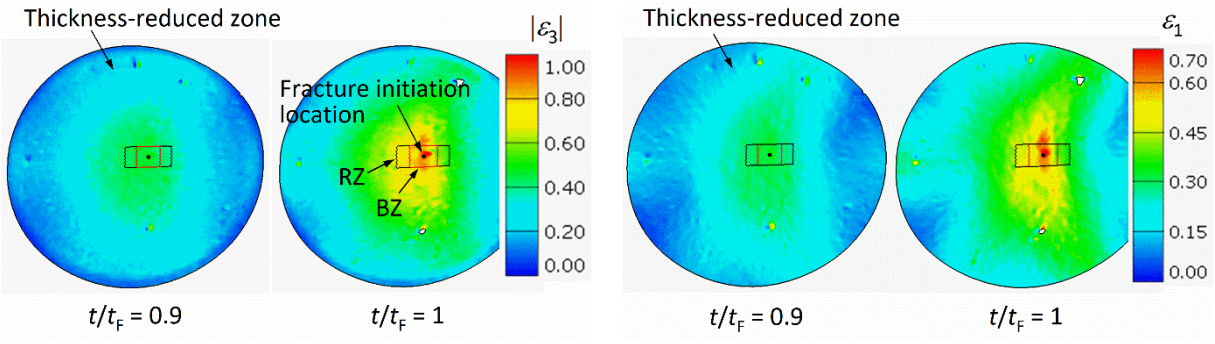

(a) (b)

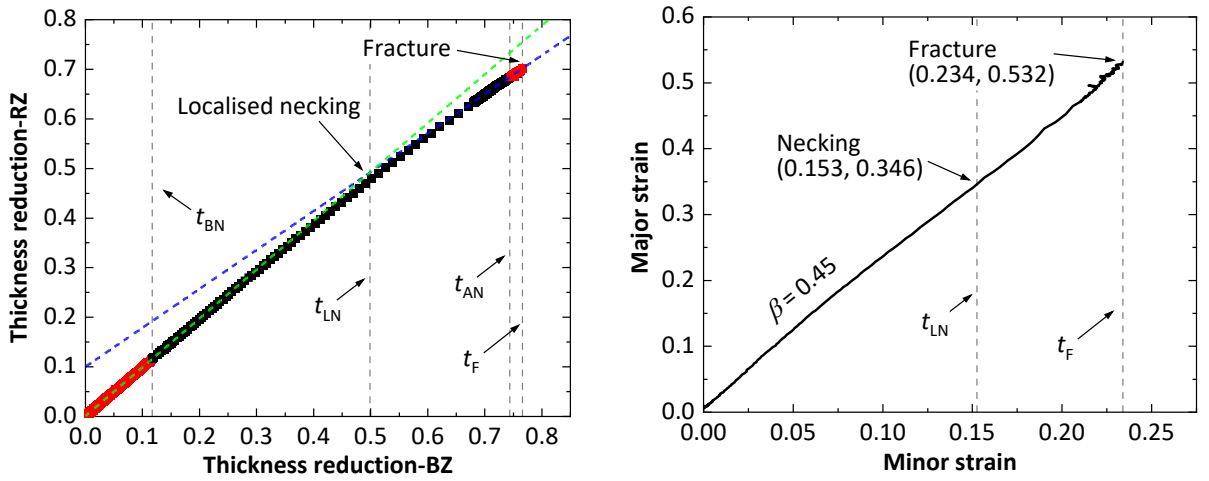

(c) (d)

Fig. 6. Determination of necking and fracture limits using the spatio-temporal method for the specimen deformed at 800 °C and 0.1 /s under equi-biaxial tension: (a) thickness reduction in specimen central region at different normalised times, (b) corresponding major strain, (c) time t_{LN} at the beginning of localised necking and time t_F at fracture, and (d) plot of major strain ε_1 versus minor strain ε_2, showing the necking and fracture limit strain pairs obtained, together with strain path.

3.2.2. Plane-strain tension

Fig. 7 shows photographs of fractured specimens obtained by testing in plane-strain tension under the five test conditions. Similarly to the tests under equi-biaxial tension, fracture took place very close to the specimen centre in all these tests. In the plane-strain case, all the cracks observed were oriented approximately in the vertical direction.

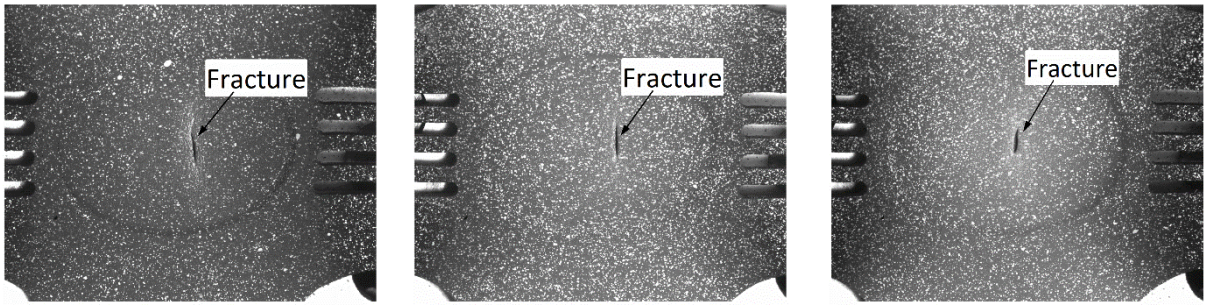

(a) (b) (c)

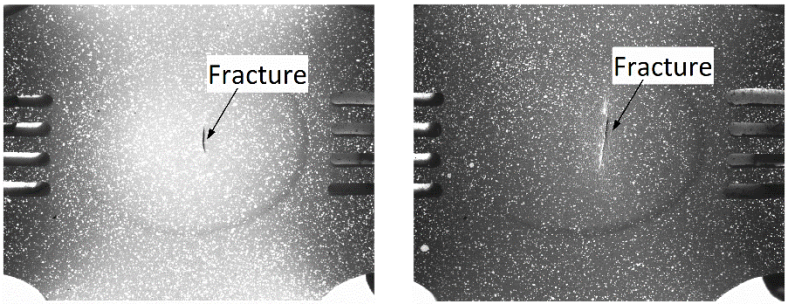

(d) (e)

Fig. 7. Fractured specimens subjected to plane-strain tension, at temperatures and strain rates of (a) 750 °C & 0.1 /s, (b) 800 °C & 0.1 /s, (c) 850 °C & 0.1 /s, (d) 800 °C & 0.02 /s and (e) 800 °C & 0.5 /s.

As above, both the necking and fracture limit strains were obtained by means of the spatio-temporal method. Fig. 8 presents results for the test at 800 °C and 0.1 /s. Figs. 8(a) and 8(b) are colour plots of thickness reduction and major strain respectively, at t/t_F = 0.9 and 1, showing zones BZ and RZ drawn around the site where fracture initiated. As in equi-biaxial tension, deformation mainly occurred close to the specimen centre. The determination of the times at which localised necking and fracture begin, t_{LN} and t_F, are shown in Fig. 8(c) and the corresponding limit strain pairs, (0.013, 0.371) and (0.028, 0.574) respectively, in Fig. 8(d). This figure also shows the strain path, which is almost linear throughout deformation with an average strain ratio β of about 0.067, very close to the ideal strain ratio β = 0 for plane-strain stretching.

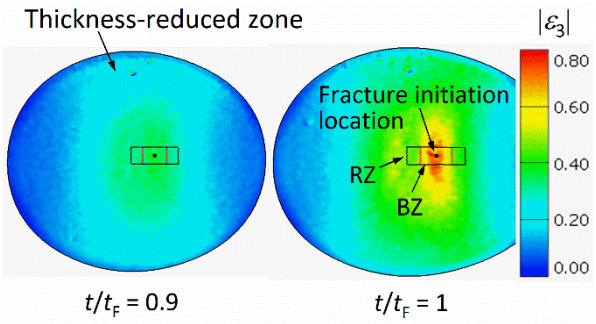

(a)

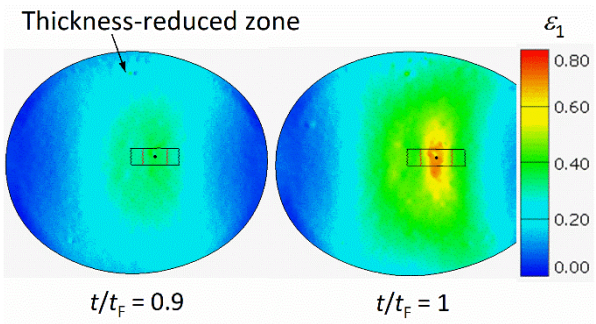

(b)

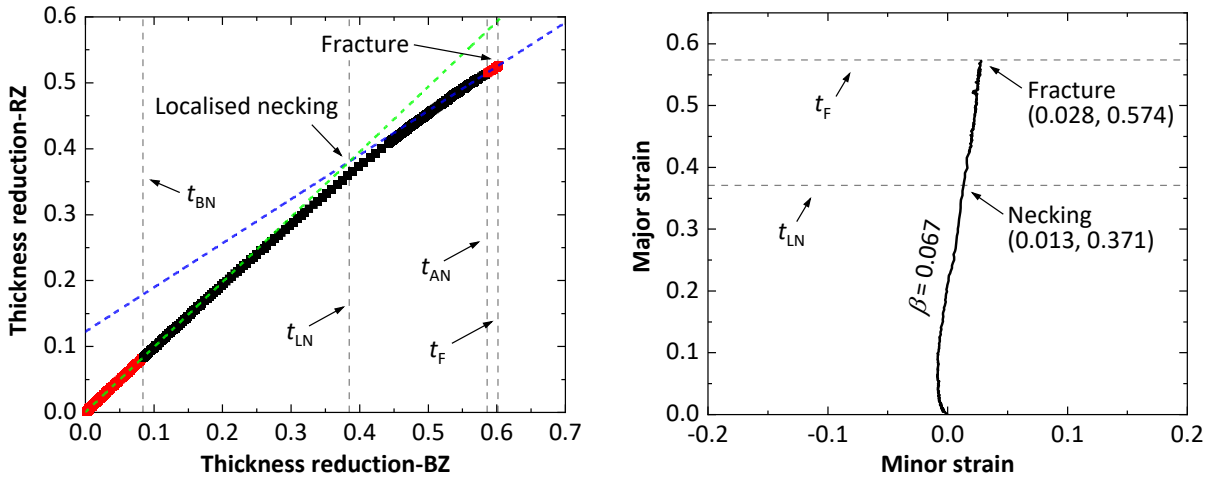

(c) (d)

Fig. 8. Determination of necking and fracture limits using the spatio-temporal method for specimen deformed at 800 °C and 0.1 /s under plane-strain tension: (a) thickness reduction in specimen centre region at different normalised times t/t_F, (b) corresponding major strain, (c) identified time t_{LN} at the beginning of localised necking and time t_F at fracture, and (d) the necking and fracture limit strain pairs obtained, together with corresponding strain path.

3.2.3. Uniaxial tension

Fig. 9 shows photographs of fractured specimens from testing in uniaxial tension under the five test conditions. Again, fracture occurred near the specimen centre within the gauge area, and cracks were oriented approximately vertically, similarly to the observations from the tests in plane-strain tension.

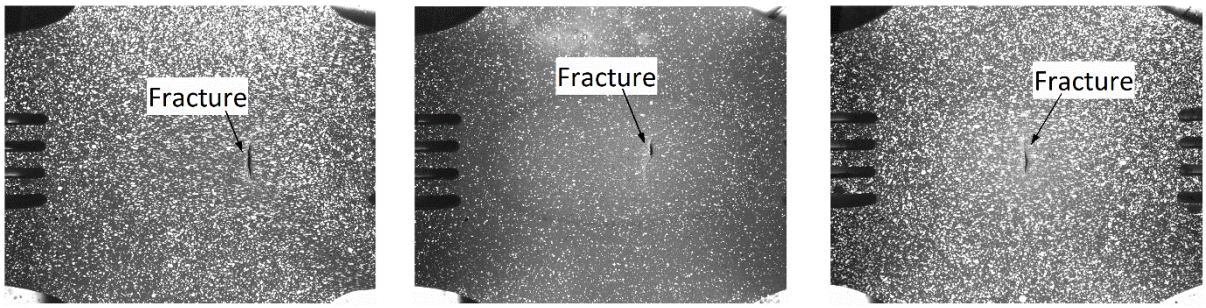

(a) (b) (c)

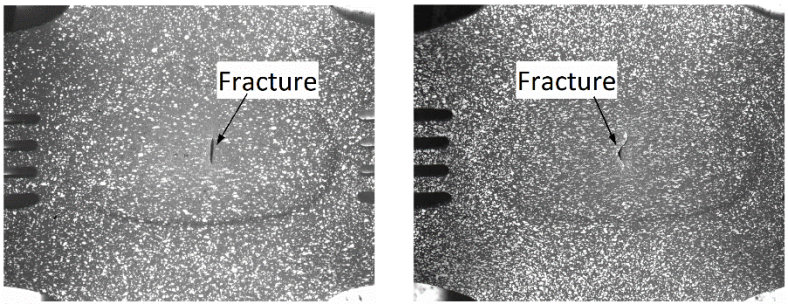

(d) (e)

Fig. 9. Fractured specimens subjected to uniaxial tension, at temperatures and strain rates of (a) 750 °C & 0.1 /s, (b) 800 °C & 0.1 /s, (c) 850 °C & 0.1 /s, (d) 800 °C & 0.02 /s and (e) 800 °C & 0.5 /s.

Fig. 10 shows the determination of the limit strains for the test in uniaxial tension at 800 °C and 0.5 /s using the methods discussed above. As above, Fig. 10(a) shows the thickness reduction at t/t_F = 0.9 and 1 and Fig. 10(b) shows the major strain; the zones BZ and RZ used for determining the limit strains are also marked in these figures. As in the equi-biaxial and plane-strain cases, deformation mainly occurred close to the specimen centre. The determination of the time at the beginning of localised necking and at fracture is shown in Fig. 10(c) and the strain path and limit strain pairs at localised necking (−0.203, 0.481) and fracture (−0.307, 0.752), are plotted in Fig. 10(d). It can be seen that the strain path is again linear, in this case having a strain ratio of about −0.40.

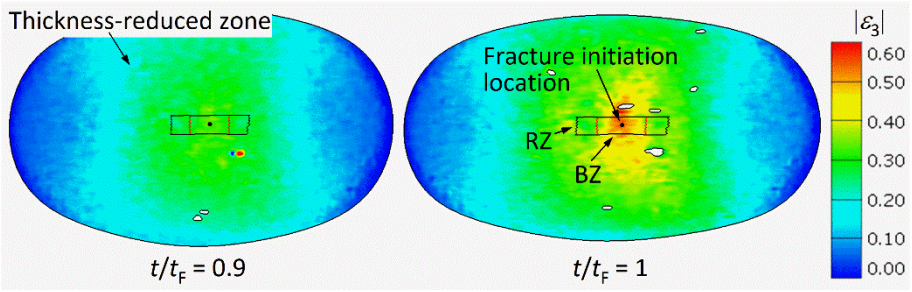

(a)

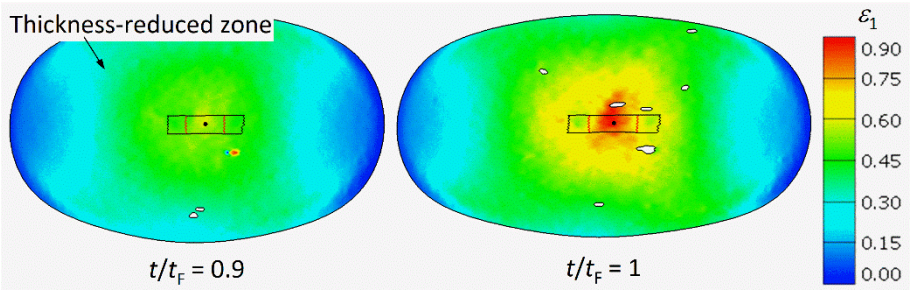

(b)

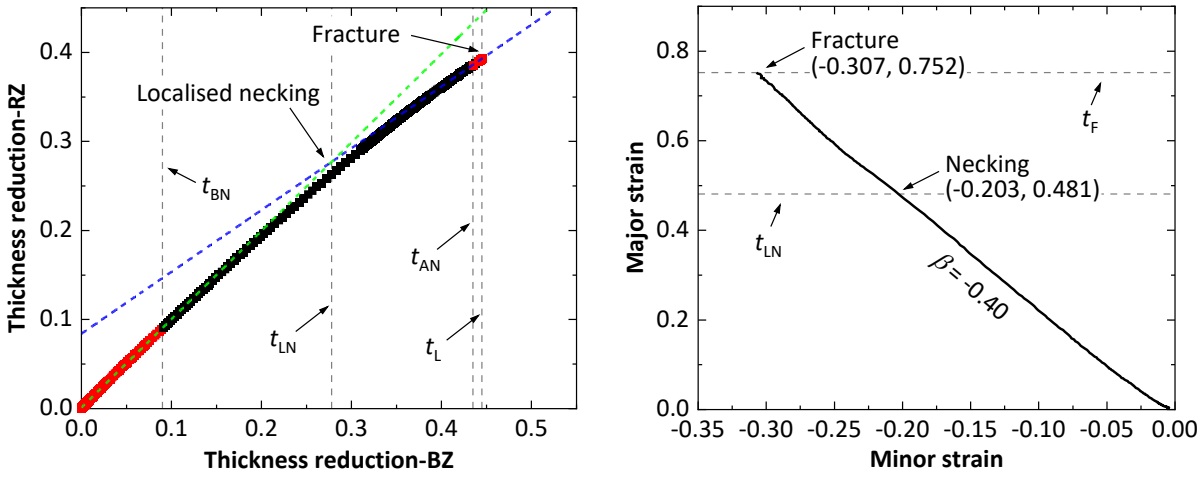

(c) (d)

Fig. 10. Determination of necking and fracture limits using the spatio-temporal method for specimen deformed at 800 °C and 0.5 /s under uniaxial tension, (a) thickness reduction in specimen centre region at different normalised times t/t_F, (b) corresponding major strain, (c) identified time t_{LN} at the beginning of localised necking and time t_F at fracture, and (d) the necking and fracture limit strain pairs obtained, together with corresponding strain path.

3.2.4. Force applied to the biaxial rig

Fig. 11 shows the measured uniaxial force applied to the biaxial tensile rig to stretch the specimens until fracture in equi-biaxial (Fig. 11(a)), plane-strain (Fig. 11(b)) and uniaxial (Fig. 11(c)) tension. As can be seen, the peak force required to stretch the specimen to fracture in a given strain state increased with increasing strain rate and with decreasing temperature. This is due to the viscoplastic nature of the material under hot stamping conditions (Zhang et al., 2020). The maximum value of the peak force in the equi-biaxial tension case was approximately 24 kN, observed in the test conducted at 800 °C & 0.5 /s (Fig. 11(a)). Under plane-strain tension conditions, the maximum value even reached approximately 27.5 kN in the test at 750 °C & 0.1 /s, as shown in Fig. 11(b), which was very close to the loading capacity of the biaxial tensile rig. This constitutes an upper limit to the size of the gauge region in the modified cruciform specimens, which are relatively small compared to the waisted specimens used in the standard Nakajima tests.

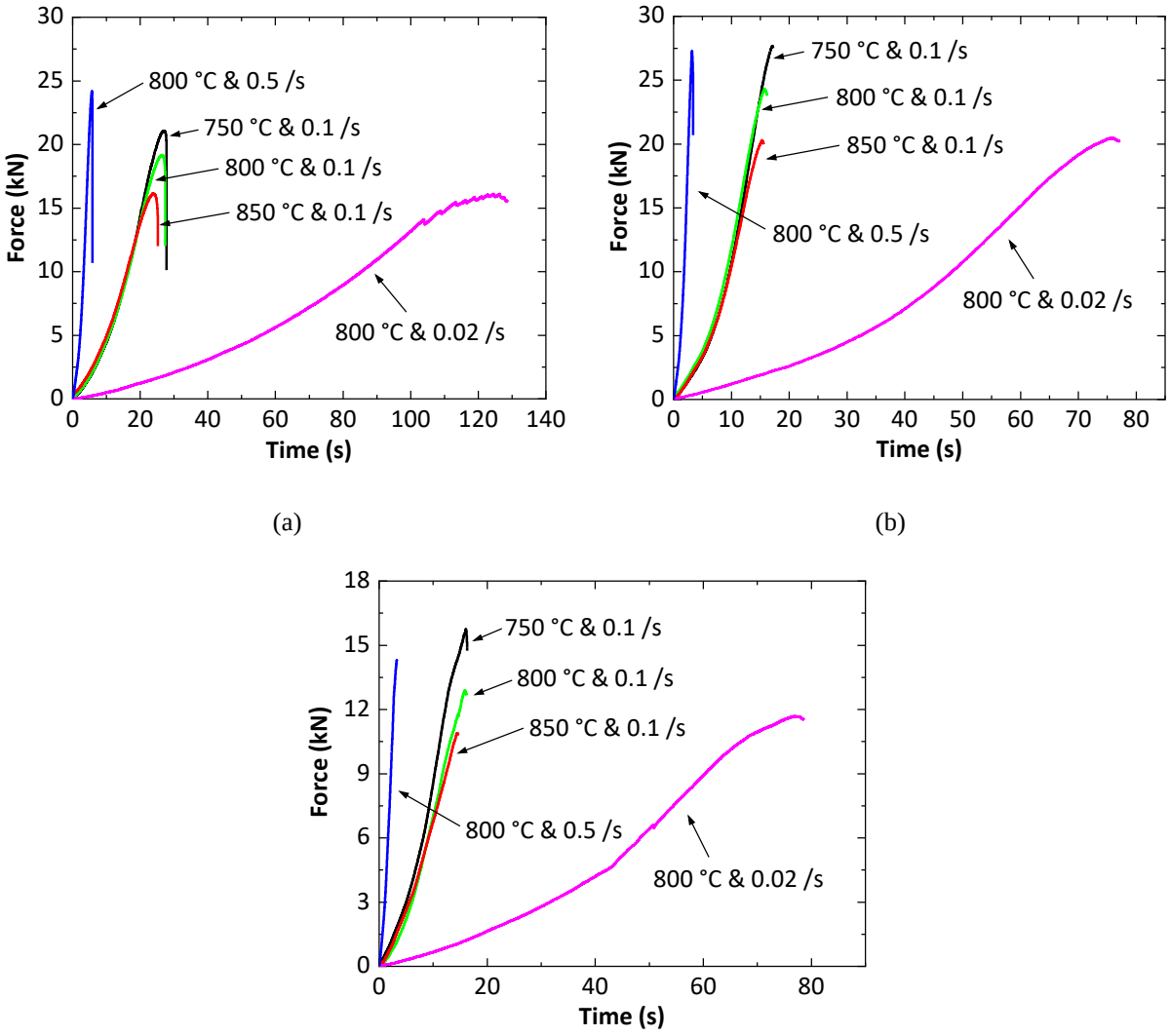

Fig. 11. Total force applied to biaxial tensile rig to stretch the boron steel cruciform specimens until fracture, at the temperatures and effective strain rates indicated, in (a) equi-biaxial tension, (b) plane-strain tension, and (c) uniaxial tension. (Note different vertical scale for (c).)

3.2.5. FLCs and FFLCs for 22MnB5 boron steel

Fig. 12 shows the collated set of limit strain pairs obtained in this study. More than one limit strain pair can be seen for certain conditions; these results represent repeat tests carried out under the same conditions. Fig. 12(a) is a plot of major strain against minor strain for data obtained at a strain rate of 0.1 /s and temperatures of 750, 800, and 850 °C, with FLCs and FFLCs generated by connecting the limit strain pairs using smooth curves for the same temperature and effective strain rate. These smooth

curves are used to guide the eye and are based on shapes observed using Nakajima testing, but further work is needed to determine the limit strains in intermediate strain states, so as to construct FLCs and FFLCs more precisely. It can be seen from Fig. 12(a) that the forming limits of the material with respect to localised necking (i.e. FLCs) and fracture (i.e. FFLCs) become higher at higher temperatures. However, this temperature effect is rather small in the temperature range investigated, especially for localised necking. For example, in plane-strain tension, the average limit major strain at localised necking at 750 °C is about 0.35, which is only 4.6% smaller than that at 800 °C, and 10.8% smaller than that at 850 °C. Temperature has a greater influence on the limit strains at fracture, but the maximum difference between average limit major strains at fracture is still less than 12%. Fig. 12(b) presents the data obtained from tests carried out at 800 °C and strain rates of 0.02, 0.1 and 0.5 /s. The forming limits are slightly higher at lower strain rates within the range investigated, but a decrease in strain rate from 0.5 to 0.02 /s has a smaller effect than an increase in temperature from 750 to 850 °C, with a maximum difference of 6.7% for necking major strain and 9.8% for fracture major strain. Furthermore, Fig. 12 demonstrates that the limit major strain values for both localised necking and fracture decrease as the strain state is varied from uniaxial to plane-strain, then change little from plane-strain to the intermediate strain state (β = ~0.45) between plane-strain and equi-biaxial.

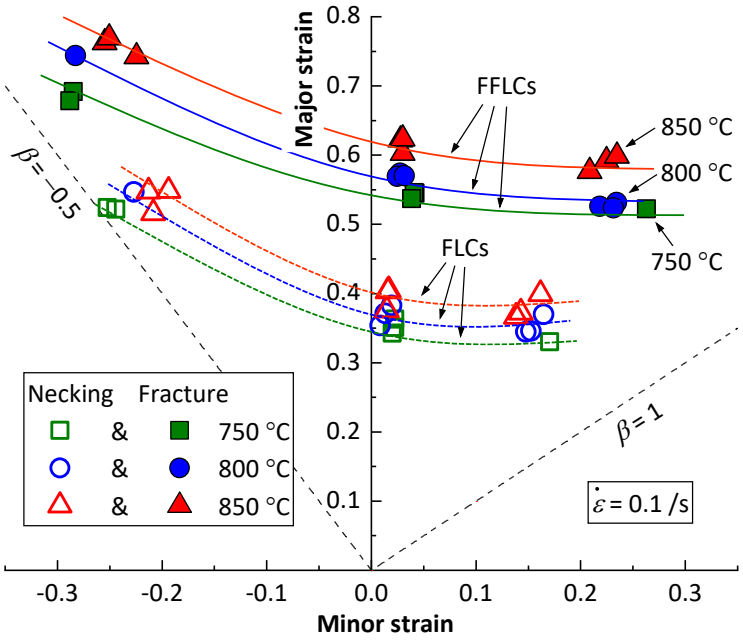

(a)

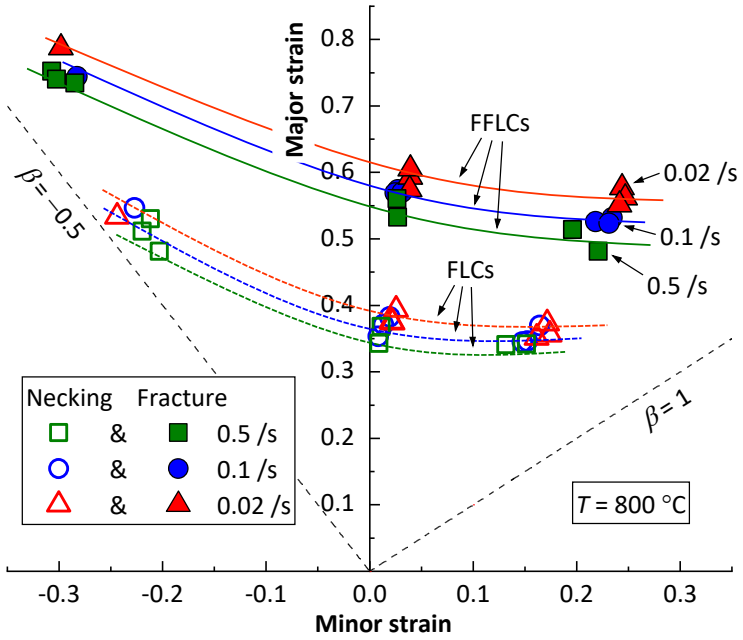

(b)

Fig. 12. Collated necking (hollow symbols) and fracture (solid symbols) limit strains for boron steel at hot stamping temperatures, and FLCs and FFLCs constructed by connecting limit strains, (a) at 0.1 /s and different temperatures of 750, 800, 850 °C, and (b) at 800 °C and different strain rates of 0.02, 0.1, 0.5 /s.

4. Discussion

4.1. Cruciform specimen design and temperature distribution

In this study, a modified cruciform specimen design and a specimen heating strategy, together with the existing biaxial tensile system, have been applied successfully to carry out biaxial testing on boron steel at hot stamping temperatures. The cruciform specimen design recently reported by Zhang et al. (2021a) has been modified to make it suitable for high-temperature applications; all modifications and the rationale behind them are described in detail in Section 2.3.1. In the modified cruciform specimens, the temperature at the centre was highest within the gauge area and the temperature difference between the centre and the perimeter of the gauge area was less than 45 °C for tests in the temperature range of 750 to 925 °C. In addition, it was demonstrated that the temperature at the specimen centre could be made to follow precisely the heat-treatment histories representative of those used in industrial hot stamping operations. For all the test conditions investigated in the current work, fracture took place very close to the centre of the cruciform specimen. This indicates the suitability of the modified cruciform specimen design and the temperature distribution within the gauge area for formability assessment. These achievements make it possible to evaluate the formability of the material at hot stamping temperatures.

However, the current cruciform specimen design has a much smaller gauge area than in the waisted Nakajima test specimens (BS EN ISO 12004, 2008). The gauge area is limited in the cruciform design because the highest total force to fracture the specimens is close to the loading capacity of the biaxial tensile rig (see Fig. 11). It would therefore be of interest, in future studies, to increase the loading capacity of the rig and enlarge the gauge zone of the cruciform specimen and compare limit strains obtained using the different cruciform specimens.

4.2. Strain path and strain state

According to Figs. 6, 8 and 10, linear strain paths were produced in all the boron steel formability tests using the modified biaxial test method. It is well known that in the standard Nakajima test, fracture should occur on the top of the dome in order to ensure nearly linear strain paths (BS EN ISO 12004, 2008). However, this is sometimes difficult to control and achieve, especially in warm or hot Nakajima tests (Min et al., 2010a). Since forming limits of sheet metals sometimes depend strongly on the linearity of strain paths (Schlosser et al., 2019), the ability of the high-temperature biaxial test method presented here to produce linear strain paths is one of the major advantages of this method for formability evaluation. In previous studies (Zhang et al., 2021a; Zhang et al., 2021c), linear strain paths were obtained in formability tests at room temperature because the fracture was initiated at the specimen centre. In the present study, the direct resistance heating method was used for formability tests at hot stamping temperatures, and the specimen design developed in (Zhang et al., 2021a) was modified to improve the uniformity of the temperature distribution and to make sure that the fracture occurred near the specimen centre, so as to obtain linear strain paths as observed. Therefore, obtaining the linear strain paths in the present study requires both an optimised specimen design and selection of an appropriate heating strategy. Furthermore, it is interesting to note that the linearity of the strain paths continued after the initiation of localised necking until fracture, i.e. the strain paths are linear throughout deformation. This differs from the observations in some formability tests at room temperature such as Nakajima tests (Mu et al., 2020) and biaxial tests (Zhang et al., 2021c), where the strain path changes to that of a plane-strain state after the beginning of localised necking. The strain path evolution after necking may be related to the specimen geometry and test conditions and further work is needed to explain the mechanisms of these different observations.

The strain ratios achieved in plane-strain and uniaxial tension, i.e. $\beta = 0.067$ and $\beta = -0.40$ (Figs. 8 and 10) are very close to the ideal strain ratios $\beta = 0$ and $\beta = -0.5$, respectively. However, in the equi-biaxial tension with a displacement ratio of 1, the strain ratio achieved is $\beta = 0.45$, considerably lower

than the ideal strain ratio β = 1 (Fig. 6(d)). In the recent study of formability evaluation at room temperature (Zhang et al., 2021c), a strain ratio smaller than the ideal value of 1 was also observed in equi-biaxial tension. However, in that case, a higher value of β = 0.78 was obtained. These results suggest that, apart from contributions from the anisotropy of the material, the relatively small strain ratio in equi-biaxial tension may be attributed to the difference of temperature distribution between the orthogonal arms, and the asymmetry of the cruciform specimen design about the diagonal directions. Intermediate strain states between $\beta = -0.40$ and $\beta = 0.45$ can be achieved by using suitable displacement ratios between −0.17 and 1, whereas to successfully obtain strain states between β = 0.45 and β = 1, the cruciform specimen design may need to be further improved to give the same geometry and temperature distribution in the vertical and horizontal arms. The other potential method to obtain the equi-biaxial strain state is to apply displacement ratios $\Delta y/\Delta x$ higher than 1 (e.g. $\Delta y/\Delta x$ = 1.2) to the cruciform specimens. This will necessitate a redesign of the biaxial tensile rig to produce those displacement ratios, and further work is needed to verify this method.

4.3. Determination of FLCs and FFLCs at hot stamping temperatures

Using the modified biaxial test method, both FLCs and FFLCs for 22MnB5 boron steel at hot stamping temperatures have been successfully determined for the first time (Fig. 12). The FLC and FFLC data determined may provide an experimental foundation for the formulation or calibration of viscoplastic constitutive equations for modelling FLCs and FFLCs, such that forming limits of the material can be predicted for industrial hot stamping applications (Park et al., 2017). According to Fig. 12, the limit major strains at localised necking in the intermediate strain state (β = 0.45) were slightly lower than those in plane strain. This differs from a conventional FLC at room temperature, in which, as reported by Hu et al. (2018) and by Basak and Panda (2019), the limit major strain in the plane-strain state has a lower value than in the other strain states. The possible reasons for this difference might be related to materials, test conditions and formability test methods. For example, a

similar phenomenon was also reported by Li et al. (2014) in formability evaluation for boron steel 22MnB5 at 800°C and by Li et al. (2020) for magnesium alloy AZ31B at 150 °C using Nakajima testing. The experimental results presented in Figs. 6(c), 8(c) and 10(c) show that the recently developed spatio-temporal method (Zhang et al., 2021b) is also applicable to high-temperature tests, enabling the necking and fracture limit strains to be determined in a single process. However, compared with those in Figs. 8(c) and 10(c), there is a relatively small difference between the slope values of the two fitted straight lines in Fig. 6(c), which may increase the experimental uncertainty associated with determining the point of intersection of the two lines. This is attributed to the fact that necking in equi-biaxial tension proceeds much faster than that in either plane-strain or uniaxial tension, as reported by Atkins (1996) and by Song et al. (2017); in equi-biaxial tension, there is only a small increase in limit major strains between the onset of localised necking and fracture. In this study, at least 20 data points were used for fitting each of the two straight lines separately, so that the experimental uncertainty was minimised.

5. Conclusions

In this study, a recently developed biaxial test method has been modified and applied for the first time to evaluate the formability, in the form of FLCs and FFLCs, of boron steel (22MnB5) sheet with a thickness of 1.5 mm at hot stamping temperatures. Biaxial tensile tests have been conducted under different forming conditions, and the necking and fracture limits have been obtained for the construction of both FLCs and FFLCs. From the study, the following conclusions can be drawn:

1) The modified biaxial test method, which comprises the modified cruciform specimen design, the biaxial tensile system combined with the direct resistance heating strategy and the spatio-temporal method, has been shown to be capable of determining limit strains at the onset of necking and fracture, leading to the possibility of constructing both FLCs and FFLCs for the material at hot stamping temperatures.

2) The FLCs and FFLCs determined are relatively insensitive to both temperature and strain rate in the ranges used, with the limit major strains varying less than 12% for temperatures between 750 and 850 °C and for strain rates between 0.02 and 0.5 /s. The limit major strain values in the plane-strain state are at least 15% lower than those in the uniaxial strain state, whereas those in the intermediate strain state (β = ~0.45) between plane-strain and equi-biaxial are very close to those in plane strain.
3) By using the modified cruciform specimen design in combination with the heating strategy for tests with target temperatures in the range of 750 to 925 °C, the temperature at the centre is highest within the gauge area and the temperature decrease from the centre of the gauge area to its perimeter could be kept to less than 45°C. Furthermore, and most importantly, the design enables the fracture to occur consistently very close to the centre of the cruciform specimen under the different testing conditions investigated.
4) Using the modified biaxial test method, linear strain paths can be produced around the fracture initiation site in the different strain states, i.e. the intermediate strain state (β = ~0.45), plane-strain and uniaxial, investigated in the present study. In addition, the strain paths remain linear, even after the formation of localised necking, up until fracture.

Acknowledgements

The authors would like to thank EPSRC for financial support (Grant no. EP/R001715/1) on "Lightform: Embedding Materials Engineering in Manufacturing with Light Alloys". R. Zhang also acknowledges the CSC Imperial Scholarship for financial support (Grant no. 201700260069).

Appendix A. Simulations of temperature distribution

Finite element (FE) simulations were performed to compute the temperature distributions in the specimens during typical hot-stamping thermal cycles. Results from these simulations were used to

modify the specimen design and to optimise the specimen dimensions so as to minimise the temperature variation within the gauge area; the final design and values are given in Fig. 3 and Table 2, respectively. For this purpose, a fully coupled thermal-electrical procedure, provided in the ABAQUS/Standard software package (SIMULIA, USA), was used to simulate resistance heating. The cruciform specimens were meshed with hexahedral elements, using a finer size of 0.5 mm in the central region and a coarser size of 1 mm in other regions, as illustrated in Fig. A1. In the simulation, a surface current was applied to the grip region connected to the positive electrode, and a zero electric potential was applied to the grip region diametrically opposite and connected to the negative electrode (Fig. A1). To simulate heat transfer in the grip regions, an interaction of the surface-to-surface contact type was defined, in which, to give agreement with experimental conditions and results, a thermal conductance of 0.1 W/(m^2·K) was found by trial and error. An initial temperature of 20 °C was applied to the cruciform specimens. The following physical properties of the boron steel were used for the simulations: density 7830 kg/m^3, electrical conductivity 6.29e+06 S/m, thermal conductivity 32 W/(m·K), specific heat capacity 712 J/(kg·K). In order to simulate a thermal cycle such as that in Fig. 1 at the specimen centre, a user subroutine UAMP, which was originally developed by Kardoulaki et al. (2014), was used to enable feedback control of the surface current using the instantaneous temperature at the specimen centre.

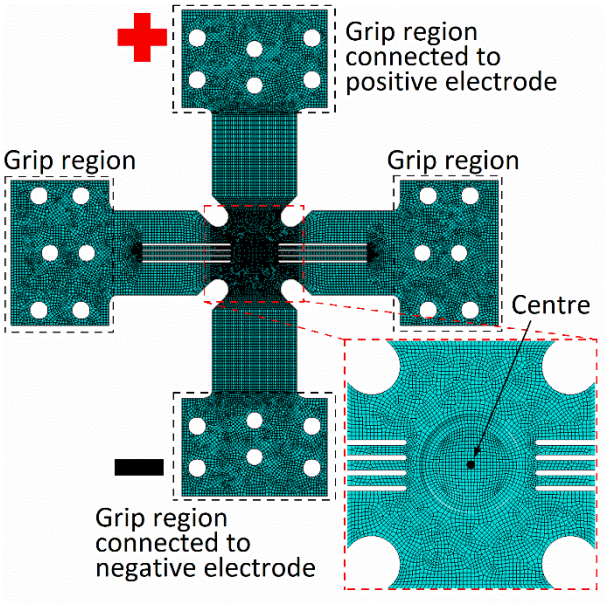

Fig. A1. FE model of the modified cruciform specimen for the computation of temperature distribution heated using direct resistance heating.

Fig. A2 shows the computed temperature distributions in the boron steel cruciform specimens, together with temperatures at the five preselected locations A-E (Fig. 3), when the temperature at the specimen centre follows the thermal cycle (Fig. 1) and reaches the soaking temperature of 925 °C (Fig. A2(a)) and the forming temperatures T_F of 850 °C (Fig. A2(b)), 800 °C (Fig. A2(c)) and 750 °C (Fig. A2(d)). In all cases, the temperature distribution is symmetrical with respect to both the horizontal and the vertical arm axes. The temperature within the gauge area was highest at the specimen centre, and decreased gradually with increasing distance from the centre. The decrease per unit distance was greater in the horizontal arm direction than in the other directions such as in the vertical and diagonal directions. Given that the locations A, B and C are on the perimeter of the gauge area, the maximum decrease within the gauge area was less than 44.3 °C. Under the other three test conditions, as shown in Figs. A2(b), A2(c), and A2(d), similar temperature distributions were produced, and the maximum temperature difference within the gauge area was less than 38.0 °C, 32.7 °C, and 28.2 °C, respectively.

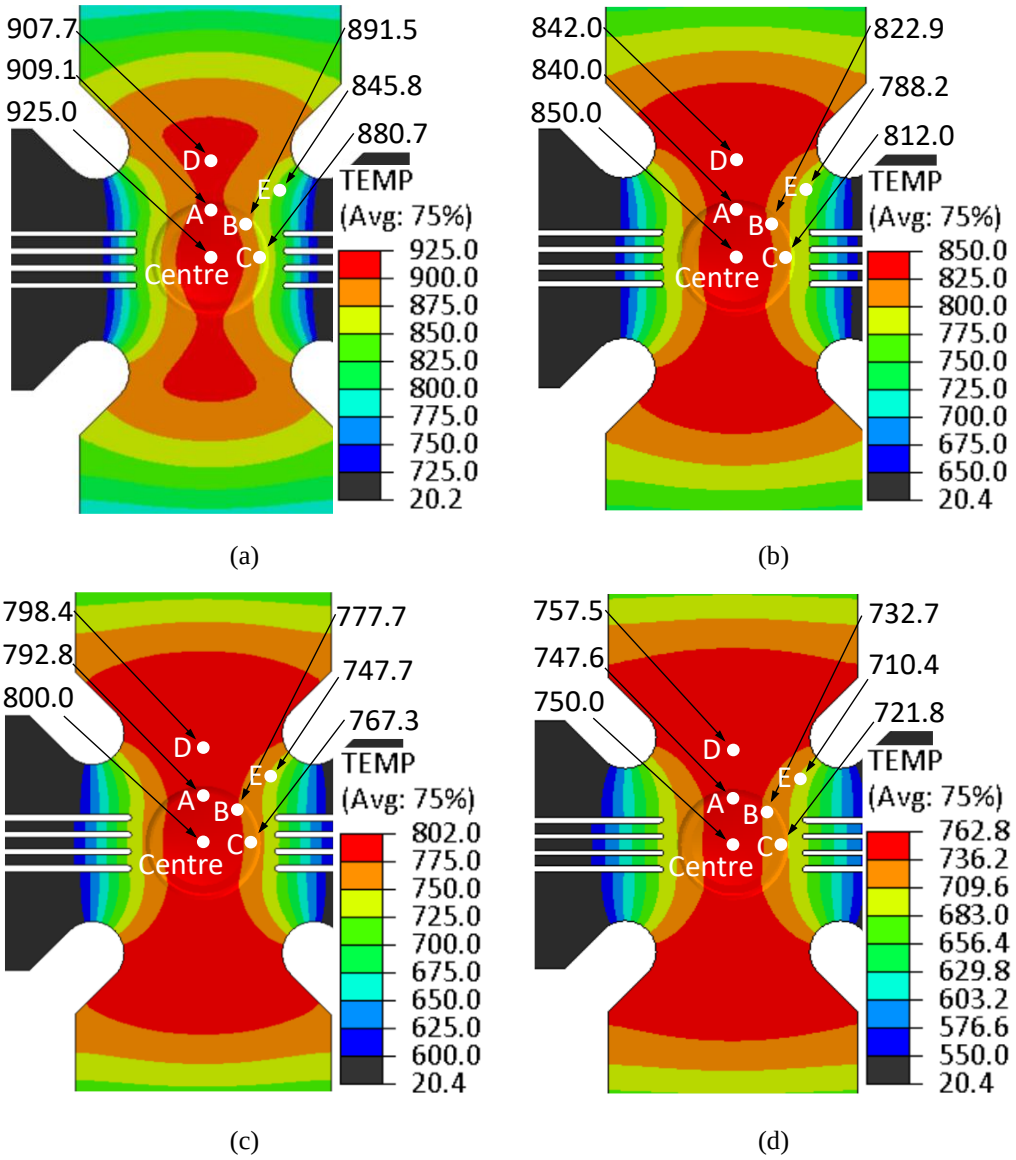

Fig. A2. Temperature distribution in the modified cruciform specimen computed using FE simulations when the temperature value (°C) at the specimen centre reaches (a) 925.0, (b) 850.0, (c) 800.0 and (d) 750.0, together with the temperature values (°C) at the locations A, B, C, D and E.

The computed temperatures at the five locations (Fig. A2) were compared with the measured values (Table 3) to quantify the difference between numerical and experimental results. The results are given in Table A1. As can be seen, there is good agreement between computation and experiment, especially at the locations A, B and C around the gauge area. For example, when the target temperature at the specimen centre is 925.0 °C, the difference between the measured and computed temperatures at the locations A, B and C is only 3.8 °C, 5.1 °C and 2.3 °C, respectively, while at the locations D and E outside the gauge area, it is 7.2 °C and 13.3 °C, respectively. It can thus be

considered that the FE simulations have been validated by experiment with respect to the temperature distributions in the specimens.

Table A1 Comparison between measured temperatures (°C), indicated by 'Exp.', and computed temperatures (°C), indicated by 'Comp.', at the locations A, B, C, D and E, for different temperatures at the specimen centre.

Specimen centre	A		B		C		D		E	
	Exp.	Comp.	Exp.	Comp.	Exp.	Comp.	Exp.	Comp.	Exp.	Comp.
925.0	912.9	909.1	896.6	891.5	883.0	880.7	914.9	907.7	859.1	845.8
850.0	838.8	840.0	819.6	822.9	806.8	812.0	845.8	842.0	786.7	788.2
800.0	790.0	792.8	770.4	777.7	758.4	767.3	801.2	798.4	741.6	747.7
750.0	740.4	747.6	721.0	732.7	710.7	721.8	757.9	757.5	696.7	710.4

In order to demonstrate the necessity for the modifications of the cruciform specimen for high-temperature use (as detailed in Section 2.3.1), temperature distribution in the cruciform specimen originally developed by Zhang et al. (2021a), was also computed using the above calibrated FE simulations and the result is shown in Fig. A3. It can be seen that the temperature at the location M within the zone N between the vertical arm notches, as indicated in Fig. A3, was highest, reaching 833.2 °C which is 33.2 °C higher than that at the specimen centre. During deformation, a combination of the higher temperature and the position of the vertical slits could cause premature fracture in the arm notches rather than in the gauge area. It is therefore necessary to make the modifications (as detailed in Section 2.3.1) to increase the temperature values at the specimen centre relative to those in the other regions, so that fracture is initiated near the specimen centre where temperature is being measured and controlled (as detailed in Section 3.2), and also, to reduce the nonuniformity of the temperature distribution within the gauge area.

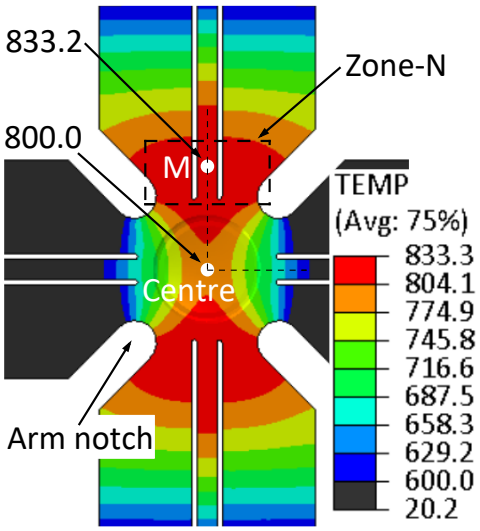

Fig. A3. Temperature distribution in the cruciform specimen originally developed by Zhang et al. (2021a), computed using the above calibrated FE simulations when the temperature value at the specimen centre reaches 800 °C. The location M within the zone N in the vertical arm notches has the highest temperature of 833.2 °C in the specimen.

References

Atkins, A., 1996. Fracture in forming. Journal of Materials Processing Technology 56, 609-618. http://dx.doi.org/10.1016/0924-0136(95)01875-1

Bachman, K., 2018. Hot-stamped parts in 2019 vehicles, https://www.thefabricator.com/stampingjournal/article/stamping/hot-stamped-parts-in-2019-vehicles

Bariani, P., Bruschi, S., Ghiotti, A., Turetta, A., 2008. Testing formability in the hot stamping of HSS. CIRP Annals - Manufacturing Technology 57, 265-268. http://dx.doi.org/10.1016/j.cirp.2008.03.049

Basak, S., Panda, S.K., 2019. Failure strains of anisotropic thin sheet metals: Experimental evaluation and theoretical prediction. International Journal of Mechanical Sciences 151, 356-374. http://dx.doi.org/10.1016/j.ijmecsci.2018.10.065

Bruni, C., Forcellese, A., Gabrielli, F., Simoncini, M., 2010. Effect of temperature, strain rate and fibre orientation on the plastic flow behaviour and formability of AZ31 magnesium alloy. Journal of Materials Processing Technology 210, 1354-1363. http://dx.doi.org/10.1016/j.jmatprotec.2010.03.025

BS EN ISO 12004, 2008. Metallic materials — Sheet and strip — Determination of forming-limit curves Part 2: Determination of forminglimit curves in the laboratory. http://dx.doi.org/10.3403/bseniso12004

BS ISO 16842, 2014. Metallic materials — Sheet and strip — Biaxial tensile testing method using a cruciform test piece. http://dx.doi.org/10.3403/30246886

Chen, L., Fang, S., Zhao, K., Xiao, R., Zhai, H., 2020. Forming limit prediction using an integrated model for 7075 aluminum alloy sheets at an elevated temperature. International Journal of Solids and Structures 202, 475-485. http://dx.doi.org/10.1016/j.ijsolstr.2020.06.030

Farhadzadeh, F., Salmani-Tehrani, M., Tajdari, M., 2018. Determining biaxial tensile stresses by fracture cruciform specimen at different temperatures and strain rates for Ti–6Al–4V alloy. Journal of the Brazilian Society of Mechanical Sciences and Engineering 40, 532. http://dx.doi.org/10.1007/s40430-018-1455-3

Goodwin, G.M., 1968. Application of strain analysis to sheet metal forming problems in the press shop, SAE Technical Paper, pp. 380-387. http://dx.doi.org/10.4271/680093

Güler, B., Efe, M., 2018. Forming and fracture limits of sheet metals deforming without a local neck. Journal of Materials Processing Technology 252, 477-484. http://dx.doi.org/10.1016/j.jmatprotec.2017.10.004

Hannon, A., Tiernan, P., 2008. A review of planar biaxial tensile test systems for sheet metal. Journal of Materials Processing Technology 198, 1-13. http://dx.doi.org/10.1016/j.jmatprotec.2007.10.015

Hu, Q., Zhang, L., Ouyang, Q., Li, X., Zhu, X., Chen, J., 2018. Prediction of forming limits for anisotropic materials with nonlinear strain paths by an instability approach. International Journal of Plasticity 103, 143-167. http://dx.doi.org/10.1016/j.ijplas.2018.01.006

Jawale, K., Duarte, J.F., Reis, A., Silva, M.B., 2018. Characterizing fracture forming limit and shear fracture forming limit for sheet metals. Journal of Materials Processing Technology 255, 886-897. http://dx.doi.org/10.1016/j.jmatprotec.2018.01.035

Karbasian, H., Tekkaya, A.E., 2010. A review on hot stamping. Journal of Materials Processing Technology 210, 2103-2118. http://dx.doi.org/10.1016/j.jmatprotec.2010.07.019

Kardoulaki, E., Lin, J., Balint, D., Farrugia, D., 2014. Investigation of the effects of thermal gradients present in Gleeble high-temperature tensile tests on the strain state for free cutting steel. The Journal of Strain Analysis for Engineering Design 49, 521-532. http://dx.doi.org/10.1177/0309324714531950

Keeler, S.P., 1965. Determination of forming limits in automotive stampings. Sheet Metal Industry 42, 683-691. http://dx.doi.org/10.4271/650535

Leotoing, L., Guines, D., Zidane, I., Ragneau, E., 2013. Cruciform shape benefits for experimental and numerical evaluation of sheet metal formability. Journal of Materials Processing Technology 213, 856-863. http://dx.doi.org/10.1016/j.jmatprotec.2012.12.013

Li, F., Fu, M., Lin, J., Wang, X., 2014. Experimental and theoretical study on the hot forming limit of 22MnB5 steel. The International Journal of Advanced Manufacturing Technology 71, 297-306. http://dx.doi.org/10.1007/s00170-013-5468-x

Li, N., Lin, J., Balint, D.S., Dean, T.A., 2016. Experimental characterisation of the effects of thermal conditions on austenite formation for hot stamping of boron steel. Journal of Materials Processing Technology 231, 254-264. http://dx.doi.org/10.1016/j.jmatprotec.2015.12.008

Li, Z., Zhou, G., Li, D., Jain, M.K., Peng, Y., Wu, P., 2020. Forming limits of magnesium alloy AZ31B sheet at elevated temperatures. International Journal of Plasticity 135. http://dx.doi.org/10.1016/j.ijplas.2020.102822

Ma, B., Wu, X., Li, X., Wan, M., Cai, Z., 2016. Investigation on the hot formability of TA15 titanium alloy sheet. Materials & Design 94, 9-16. http://dx.doi.org/10.1016/j.matdes.2016.01.010

Marciniak, Z., Kuczyński, K., 1967. Limit strains in the processes of stretch-forming sheet metal. International Journal of Mechanical Sciences 9, 609-620. http://dx.doi.org/10.1016/0020-7403(67)90066-5

Merklein, M., Lechler, J., 2006. Investigation of the thermo-mechanical properties of hot stamping steels. Journal of Materials Processing Technology 177, 452-455. http://dx.doi.org/10.1016/j.jmatprotec.2006.03.233

Merklein, M., Wieland, M., Lechner, M., Bruschi, S., Ghiotti, A., 2016. Hot stamping of boron steel sheets with tailored properties: A review. Journal of Materials Processing Technology 228, 11-24. http://dx.doi.org/10.1016/j.jmatprotec.2015.09.023

Min, J., Lin, J., Cao, Y., Bao, W., Lu, Z., 2010a. Effect of necking types of sheet metal on the left-hand side of forming limit diagram. Journal of Materials Processing Technology 210, 1070-1075. http://dx.doi.org/10.1016/j.jmatprotec.2010.02.018

Min, J., Lin, J., Li, J., Bao, W., 2010b. Investigation on hot forming limits of high strength steel 22MnB5. Computational Materials Science 49, 326-332. http://dx.doi.org/10.1016/j.commatsci.2010.05.018

Min, J., Stoughton, T., Carsley, J., Lin, J., 2017a. A method of detecting the onset of localized necking based on surface geometry measurements. Experimental Mechanics 57, 521-535. http://dx.doi.org/10.1007/s11340-016-0232-4

Min, J., Stoughton, T.B., Carsley, J.E., Lin, J., 2017b. An improved curvature method of detecting the onset of localized necking in Marciniak tests and its extension to Nakazima tests. International Journal of Mechanical Sciences 123, 238-252. http://dx.doi.org/10.1016/j.ijmecsci.2017.02.011

Mu, L., Jia, Z., Ma, Z., Shen, F., Sun, Y., Zang, Y., 2020. A theoretical prediction framework for the construction of a fracture forming limit curve accounting for fracture pattern transition. International Journal of Plasticity 129. http://dx.doi.org/10.1016/j.ijplas.2020.102706

Nakazima, K., Kikuma, T., Hasuka, K., 1968. Study on the formability of steel sheets. Yamata Technical Report, 8517-8530

Palumbo, G., Sorgente, D., Tricarico, L., 2008. The design of a formability test in warm conditions for an AZ31 magnesium alloy avoiding friction and strain rate effects. International Journal of Machine Tools and Manufacture 48, 1535-1545. http://dx.doi.org/10.1016/j.ijmachtools.2008.06.010

Park, N., Huh, H., Lim, S.J., Lou, Y., Kang, Y.S., Seo, M.H., 2017. Fracture-based forming limit criteria for anisotropic materials in sheet metal forming. International Journal of Plasticity 96, 1-35. http://dx.doi.org/10.1016/j.ijplas.2016.04.014

Raghavan, K., 1995. A simple technique to generate in-plane forming limit curves and selected applications. Metallurgical and Materials Transactions A 26, 2075-2084. http://dx.doi.org/10.1007/bf02670679

Schlosser, F., Signorelli, J., Leonard, M., Roatta, A., Milesi, M., Bozzolo, N., 2019. Influence of the strain path changes on the formability of a zinc sheet. Journal of Materials Processing Technology. http://dx.doi.org/10.1016/j.jmatprotec.2019.03.026

Shao, Z., Li, N., Lin, J., Dean, T., 2016. Development of a new biaxial testing system for generating forming limit diagrams for sheet metals under hot stamping conditions. Experimental Mechanics 56, 1489-1500. http://dx.doi.org/10.1007/s11340-016-0183-9

Song, X., Leotoing, L., Guines, D., Ragneau, E., 2017. Characterization of forming limits at fracture with an optimized cruciform specimen: Application to DP600 steel sheets. International Journal of Mechanical Sciences 126, 35-43. http://dx.doi.org/10.1016/j.ijmecsci.2017.03.023

Turetta, A., Bruschi, S., Ghiotti, A., 2006. Investigation of 22MnB5 formability in hot stamping operations. Journal of Materials Processing Technology 177, 396-400. http://dx.doi.org/10.1016/j.jmatprotec.2006.04.041

Wang, K., Carsley, J.E., He, B., Li, J., Zhang, L., 2014. Measuring forming limit strains with digital image correlation analysis. Journal of Materials Processing Technology 214, 1120-1130. http://dx.doi.org/10.1016/j.jmatprotec.2014.01.001

Xiao, R., 2019. A review of cruciform biaxial tensile testing of sheet metals. Experimental Techniques 43, 1-20. http://dx.doi.org/10.1007/s40799-018-00297-6

Xiao, R., Li, X.-X., Lang, L.-H., Chen, Y.-K., Yang, Y.-F., 2016. Biaxial tensile testing of cruciform slim superalloy at elevated temperatures. Materials & Design 94, 286-294. http://dx.doi.org/10.1016/j.matdes.2016.01.045

Xiao, R., Li, X.-X., Lang, L.-H., Song, Q., Liu, K.-N., 2017. Forming limit in thermal cruciform biaxial tensile testing of titanium alloy. Journal of Materials Processing Technology 240, 354-361. http://dx.doi.org/10.1016/j.jmatprotec.2016.10.016

Zhang, R., Shao, Z., Lin, J., Dean, T.A., 2020. Measurement and analysis of heterogeneous strain fields in uniaxial tensile tests for boron steel under hot stamping conditions. Experimental Mechanics 60, 1289-1300. http://dx.doi.org/10.1007/s11340-020-00658-6

Zhang, R., Shao, Z., Shi, Z., Dean, T.A., Lin, J., 2021a. Effect of cruciform specimen design on strain paths and fracture location in equi-biaxial tension. Journal of Materials Processing Technology 289. http://dx.doi.org/10.1016/j.jmatprotec.2020.116932

Zhang, R., Shi, Z., Shao, Z., Dean, T.A., Lin, J., 2021b. A novel spatio-temporal method for determining necking and fracture strains of sheet metals. International Journal of Mechanical Sciences 189. http://dx.doi.org/10.1016/j.ijmecsci.2020.105977

Zhang, R., Shi, Z., Shao, Z., Yardley, V.A., Lin, J., Dean, T.A., 2021c. Biaxial test method for determination of FLCs and FFLCs for sheet metals: validation against standard Nakajima method. International Journal of Mechanical Sciences 209. http://dx.doi.org/10.1016/j.ijmecsci.2021.106694

Zidane, I., Guines, D., Leotoing, L., Ragneau, E., 2010. Development of an in-plane biaxial test for forming limit curve (FLC) characterization of metallic sheets, Measurement Science and Technology, p. 055701. http://dx.doi.org/10.1088/0957-0233/21/5/055701